Mathematics in Engineering, 5(3): 1–19.
DOI: 10.3934/mine.2023051
Received: 13 October 2021
Revised: 17 July 2022
Accepted: 16 August 2022
Published: 24 August 2022

http://www.aimspress.com/journal/mine

*Research article*

# Oldroyd 6-constant Electro-magneto-hydrodynamic fluid flow through parallel micro-plates with heat transfer using Darcy-Brinkman-Forchheimer model: A parametric investigation

**M. M. Bhatti[1,*] and Efstathios E. Michaelides[2]**

[1] College of Mathematics and Systems Science, Shandong University of Science and Technology, Qingdao 266590, Shandong, China
[2] Department of Engineering, TCU, Fort Worth, TX, USA

* **Correspondence:** Email: mmbhatti@sdust.edu.cn, mubashirme@hotmail.com.

**Abstract:** The focus of the article is the electro-magneto-hydrodynamics of an Oldroyd 6-constants fluid flow through parallel micro-plates with heat transfer. The medium between the micro-plates is porous and we use the Darcy-Brinkman-Forchheimer model for it. Numerical calculations, using the shooting method, were performed to solve the non-linear equations that emanate from the modeling. The results for the velocity mechanism, the Nusselt number and the temperature distribution are graphically shown. The analysis of the problem focuses on the effects of several fluid and heat transfer parameters, such as the Hartmann number, the Brinkmann number, the Darcy-Brinkman-Forchheimer parameter, the Darcy parameter, the viscous dissipation, and the Joule heating coefficient.

**Keywords:** Oldroyd 6-constant fluid; heat transfer; Darcy-Brinkman-Forchheimer model; parallel micro-plates; Electro-magneto-hydrodynamic (EMHD); mixed convection

## 1. Introduction

Several research studies have been accomplished recently on the heat transfer through microporous media and micro-channels with applications in thermal control in radiators, heat pipes, and microelectronics. Micro-channel systems can provide efficient heat removal at substantially smaller dimensions for cooling systems in aerospace engineering [1]. The use of micro-radiators for

thermal control enables the reduction of the maximum temperature and temperature gradients on the equipment when subjected to large heat fluxes [1]. Heat transfer mechanisms are becoming increasingly important in the modeling of several other applications including magnetic fluid power production [2], geophysical flows, and nuclear reactor cooling [3]. Heat transfer fluid flow through a porous media is also associated with several engineering applications in nuclear waste disposal systems, thermal energy transfer, and thermal management [4]. The subjects of heat transfer and flow in porous media also play an important role in the energy sector, including electro-kinetic energy conversion devices, hydrogen storage systems, shale reservoirs, and membrane-based water desalination with reverse osmosis.

Given its scientific and engineering significance, many researchers investigated heat transfer in various geometric domains and for various fluid models. Moradi et al. [5] investigated heat transfer over a porous medium using a double tube filled with water-based MWCNT nanofluids. Natural convection and heat transfer with a fluid via a coarse-grained permeable medium were investigated by Ataei-Dadavi et al. [6]. Pandya et al. [7] reviewed the heat transfer effectiveness for plate heat exchangers with nanofluids. Miri, Joibary and Siavashi [8] explored the role of Reynolds asymmetry and the use of porous media in a counter-flow dual-pipe heat exchanger to improve the heat transfer. Zhang et al. [9] used the Darcy–Brinkman–Forchheimer model for porous media to investigate the bioconvection flow over a permeable Riga plate. Also, Selimefendigil and Oztop [10] investigated the impact of nanofluids and dual porous layers in order to evaluate the heat transfer from a plate using impinging flow single-jets and multi-jets.

Heat transfer with magnetic fields is technologically important because of its numerous applications in the metallurgical industry (fluid metal flows), micro-pump flows, biological flows, and medicinal uses. In particular the electro-magneto-hydrodynamics micro-pump has attracted the attention of several researchers, because of its possible uses in microfluidic systems [11,12]. Magnetic fields generate the Lorentz force by the interactions of an externally induced electrical current in channel filled with electrically conductive fluids [13–15]. The effects of, viscous dissipation, joule heating, and thermal properties on EMHD fluid flow over a microchannel with constant heat flux were discussed by Chakraborty et al. [16]. Sarkar et al. [17] investigated the behavior of EMHD flow towards a microchannel when it was subjected to slip and electro-kinetic phenomena. Rashid et al. [18] studied the effects of EMHD and permeability on the fluid flow across a corrugated microchannel with varying viscosity. Reza et al. [19,20] investigated a third-grade fluid flow in a microchannel with EMHD and porous effects. Obalalu et al. [21] explored the effect of phase change heat transfer with a non-Newtonian EMHD nanofluid with activation energy and chemical reactions.

The main objective of this research study is to investigate the Oldroyd 6-constant, Electro-magneto-hydrodynamic fluid flow, across parallel and porous micro-plates with heat transfer, using the Darcy-Brinkman-Forchheimer model. This investigation is motivated by their fundamental importance in industrial engineering applications as well as their value for experimental purposes. Flows in microfluidic channels are also relevant in a variety of sectors [22,23], including biomedical and biochemical processes, heat exchange due to surface forces and physical particle separation. The fluid flow in the stated field is efficiently controlled by using electric fields, pressure gradients, magnetic fields, or appropriate combinations of these driving forces. The EMHD micro-pump is one of the several pumping concepts that has use in micro-fluidics systems. Because the operating concept of the EMHD micro-pump is based on the Lorentz force (created by the interaction of an externally imposed electric current along the channel with ferrofluid with a transverse magnetic field orthogonal to the current) [24].

In addition, the Oldroyd 6-constant fluid (non-Newtonian) has a number of industrial uses. Several fluid models, including Oldroyd's, have been presented in recent years. This model incorporates the elastic and memory effects that dilute solutions demonstrate. Most of the Oldroyd-B fluid models available in the literature [25,26] are confined to 3-constant models, and, hence, cannot cover the full characteristics of viscoelastic flows. This is why we chose the Oldroyd 6-constant fluid model to investigate its properties. After employing the assumptions to the mathematical modeling, the governing differential equations of the model are nonlinear and coupled. Because of this, numerical simulations are carried out using the shooting the method with the *Mathematica* software. When compared with other similar approaches, the shooting method delivers results quickly with simple computations. Results are presented for the velocity profile, the Nusselt number, and the temperature distributions for all the important to the flow parameters.

## 2. Mathematical and physical formulation of the Oldroyd 6-constant fluid

Consider an electrically conducting Oldroyd 6-constant [27] incompressible fluid that moves through parallel micro-plates under the influence of electro-magnetic forces. The fluid is moving through a porous medium. To investigate the behavior of the Oldroyd 6-constant fluid through the porous medium, the Darcy-Brinkman-Forchheimer model is used. A system of rectangular coordinates is selected such as $\tilde{x}-$ and $\tilde{z}-$ are assigned along the tangential direction on the charged plates, while the $\tilde{y}-$ axis is assigned along the perpendicular direction, as shown in Figure 1.

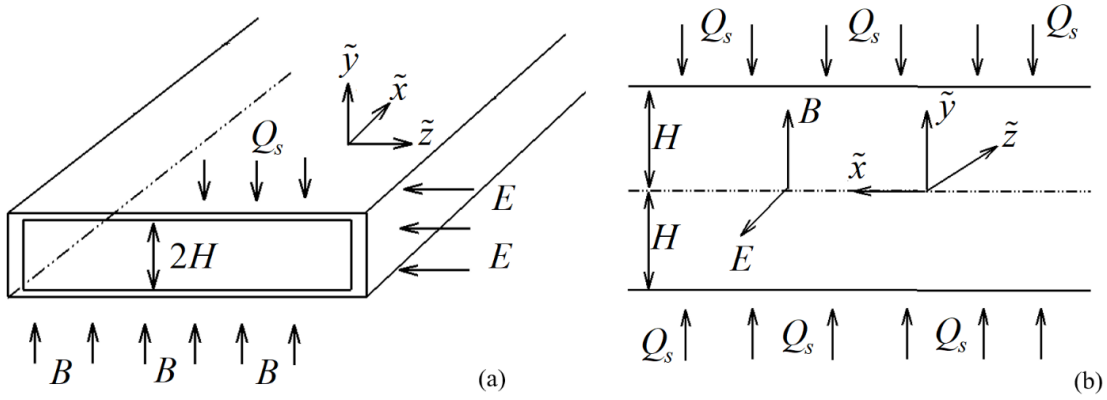


**Figure 1.** Geometrical arrangements of an EMHD micro-pump between two parallel micro-plates. (a) Three-dimensional position; (b) Two-dimensional position.

Due to the presence of electrical field $\vec{E}$ along the $\tilde{z}-$axis in the transverse direction, and the homogenously applied magnetic field $\vec{B}$ along the $\tilde{y}-$axis, a magnetic Lorentz force is generated which acts along the $\tilde{x}-$ axis. The magnetic Reynolds number is assumed to be very small and, therefore, all other effects of magnetism are neglected except for the Lorentz force. The length of the micro-channel is denoted by $L$ along the $\tilde{x}-$ axis, the width is denoted by $W$, and the height of the micro-channel is denoted by $2H$ (typically its range is $100-200\mu m$). The length of the microchannel is much larger than the height and the width, that is $L>>2H$ and $L>>W$. According to these assumptions, the two-dimensional micro-channel Oldroyd 6-constant fluid flow is reduced to a one-dimensional steady-state flow for which the velocity is independent of $\tilde{z}$. The continuity equation

for this flow is:

$$\nabla \cdot \vec{V} = 0, \tag{1}$$

Using Darcy-Brinkman-Forchheimer model and body forces, the momentum equation becomes:

$$\rho \frac{\mathrm{d}\vec{V}}{\mathrm{d}\tilde{t}} = \nabla \cdot \xi - \nabla \cdot p + B_f - \frac{\rho c_F}{K^{1/2}} \left|\vec{V}\right| \vec{V} - \frac{\mu}{K} \vec{V} + \rho g \beta \left(\tilde{T}_m - \tilde{T}_s\right), \tag{2}$$

where $\xi$ is the stress tensor of the Oldroyd 6-constant fluid, $g$ is the gravity, $B_f$ is the body force, $p$ is the pressure, $\beta$ the thermal expansion coefficient, $K$ is the permeability of the porosity, $c_F$ is the Forchheimer coefficient, $\rho$ is the density, $\tilde{t}$ is the time, and $\tilde{T}_m$ and $\tilde{T}_s$ are the average temperature and the surface temperature. The body force is the induced Lorentz force, defined as follows [28]:

$$B_f = \vec{J} \times \vec{B}, \tag{3}$$

Where $\vec{J}$ is the vector that represents the local ion current density and is given by the expression:

$$\vec{J} = \sigma \left[\vec{V} \times \vec{B} + \vec{E}\right], \tag{4}$$

where $\sigma$ represents the electrical conductivity, $\vec{B}$ the magnetic field, and $\vec{E}$ the electric field.

The stress tensor of the Oldroyd 6-constant fluid is expressed by the following equation:

$$\left.\begin{aligned} &\xi + \lambda_1 \frac{D\xi}{D\tilde{t}} + \frac{\lambda_3}{2}\left(\xi \vec{R}_1 + \vec{R}_1 \xi\right) + \frac{\lambda_5}{2}\left(\mathrm{tr}\xi\right)\vec{R}_1 = \mu\left(\vec{R}_1 + \lambda_2 \frac{D\vec{R}_1}{D\tilde{t}} + \lambda_4 \vec{R}_1^2\right), \\ &\vec{R}_1 = \vec{L} + \vec{L}^T, \quad \vec{L} = \mathrm{grad}\vec{V}, \end{aligned}\right] \tag{5}$$

Where $\vec{R}_1$ the first Rivlin-Erickson tensor, $\lambda_1, \lambda_2, \lambda_3, \lambda_4, \lambda_5$ are constants of the material, and $\mu$ is the viscosity of the fluid. The total derivative, $D/D\tilde{t}$ is defined as follows:

$$\frac{D(\bullet)}{D\tilde{t}} = \frac{\mathrm{d}(\bullet)}{\mathrm{d}\tilde{t}} - (\bullet)\vec{L}^T - L(\bullet), \tag{6}$$

Where $\frac{\mathrm{d}}{\mathrm{d}\tilde{t}}$ denotes the material derivative. The detailed derivation of Eqs (5) and (6) are presented in the Appendix.

The energy equation for this fluid, which is subjected to viscous dissipation and Joule heating effects is:

$$\rho S_h \frac{\mathrm{d}\tilde{T}}{\mathrm{d}\tilde{t}} - \frac{\vec{J} \cdot \vec{J}}{\sigma} = \xi : \mathrm{grad}\ \vec{V} + \frac{\rho c_F}{K^{1/2}} \left|\vec{V}\right|^2 \vec{V} + \frac{\mu}{K} \vec{V}^2 - \nabla \cdot \vec{Q}, \tag{7}$$

where the symbol ":" indicates the tensorial product, $\tilde{T}$ represents the temperature, $S_h$ denotes the specific heat, and $\vec{Q}$ is the heat flux vector.

For the chosen geometry shown in Figure 1, the velocity vector is defined by the following equation:

$$\vec{V} = \left[\bar{u}\left(\tilde{y}\right), 0, 0\right]. \tag{8}$$

Substituting Eq (5) in Eq (2), we obtain:

$$\frac{\partial p}{\partial \tilde{x}} = \frac{\mathrm{d}\xi_{\tilde{x}\tilde{y}}}{\mathrm{d}\tilde{y}} - \sigma B^2 \bar{u} + \sigma BE - \frac{\mu}{K}\bar{u} - \frac{\rho c_F}{K^{1/2}}\bar{u}^2 + \rho\beta g\left(\tilde{T}_m - \tilde{T}_s\right), \tag{9}$$

$$\frac{\partial p}{\partial \tilde{y}} = \frac{\partial \xi_{\tilde{y}\tilde{y}}}{\partial \tilde{y}}, \tag{10}$$

$$\frac{\partial p}{\partial \tilde{z}} = 0. \tag{11}$$

The pressure function only depends on the $\tilde{y}$ coordinates. Therefore, we obtain the following expression for the momentum equation:

$$\mu\frac{\mathrm{d}}{\mathrm{d}\tilde{y}}\left[\frac{\frac{\mathrm{d}\bar{u}}{\mathrm{d}\tilde{y}} + \beta_1\left(\frac{\mathrm{d}\bar{u}}{\mathrm{d}\tilde{y}}\right)^3}{1 + \beta_2\left(\frac{\mathrm{d}\bar{u}}{\mathrm{d}\tilde{y}}\right)^2}\right] - \sigma B^2\bar{u} + \sigma BE - \frac{\mu}{K}\bar{u} - \frac{c_F\rho}{K^{1/2}}\bar{u}^2 + \rho\beta g\left(\tilde{T}_m - \tilde{T}_s\right) = 0, \tag{12}$$

where $\beta_1 = \lambda_2\lambda_1 - \left(\lambda_4 - \lambda_2\right)\left(\lambda_5 + \lambda_3\right), \beta_2 = \lambda_3\lambda_1 - \left(\lambda_3 - \lambda_1\right)\left(\lambda_5 + \lambda_3\right)$ are derived from Eq (5).

The boundary conditions of the flow are:

$$\bar{u}\left(\tilde{y}\right) = 0, \qquad \tilde{y} = \pm H, \tag{13}$$

The governing equations of this model may be cast in dimensionless form using the following dimensional parameters:

$$\begin{aligned} &Da = \frac{H^2}{K}, F = \frac{c_f H}{\sqrt{K}}, u = \frac{\bar{u}}{\upsilon / H}, \xi_1 = \frac{\beta_1 \upsilon^2}{H^4}, \xi_2 = \frac{\beta_2 \upsilon^2}{H^4}, T = \frac{\tilde{T}\left(\tilde{x}, \tilde{y}\right) - \tilde{T}_s\left(\tilde{x}\right)}{\tilde{T}_m\left(\tilde{x}\right) - \tilde{T}_s\left(\tilde{x}\right)} \\ &Ha^2 = \frac{\sigma}{\mu}B^2H^2, E_1 = \frac{E\sigma H^2 B}{(\upsilon / H)\mu}, y = \frac{\tilde{y}}{H}, Gr = \frac{\beta g H^3\left(T_m - T_s\right)}{\upsilon^2}, \end{aligned} \tag{14}$$

Where, $\upsilon$ represents the kinematic viscosity of the fluid, $Ha$ is the Hartmann number, $T$ is the dimensionless temperature, $E_1$ is a dimensionless parameter related to the electric strength, $Da$ is the Darcy parameter and represents the porosity, $Gr$ is the thermal Grashof number, $F$ represents the Forchheimer number, which accounts for the non-Darcian effects of the porous medium and its range is from 0 to $\infty$.

Accordingly, Eq (12) becomes in dimensionless form:

$$\frac{\mathrm{d}^2u}{\mathrm{d}y^2}+\left(3\xi_1-\xi_2\right)\frac{\mathrm{d}^2u}{\mathrm{d}y^2}\left(\frac{\mathrm{d}u}{\mathrm{d}y}\right)^2+\xi_1\xi_2\frac{\mathrm{d}^2u}{\mathrm{d}y^2}\left(\frac{\mathrm{d}u}{\mathrm{d}y}\right)^4-\left(Ha^2u-E_1+Dau+Fu^2-GrT\right)\left[1+\xi_2\left(\frac{\mathrm{d}u}{\mathrm{d}y}\right)^2\right]^2=0, \tag{15}$$

The boundary conditions in dimensionless form are simplified as follows:

$$u\left(y\right)=0,\quad y=\pm1, \tag{16}$$

The EMHD fluid's energy equation is as follows:

$$\rho S_h\bar{u}\frac{\partial\tilde{T}}{\partial\tilde{x}}=T_c\left(\frac{\partial^2\tilde{T}}{\partial\tilde{x}^2}+\frac{\partial^2\tilde{T}}{\partial\tilde{y}^2}\right)+\mu\left(\frac{\mathrm{d}\bar{u}}{\mathrm{d}\tilde{y}}\right)\frac{\left[\frac{\mathrm{d}\bar{u}}{\mathrm{d}\tilde{y}}+\beta_1\left(\frac{\mathrm{d}\bar{u}}{\mathrm{d}\tilde{y}}\right)^3\right]}{\left[1+\beta_2\left(\frac{\mathrm{d}\bar{u}}{\mathrm{d}\tilde{y}}\right)^2\right]}+\sigma\left(E^2+B^2\bar{u}^2-2EB\bar{u}\right)+\frac{\rho c_F}{K^{1/2}}\bar{u}^3+\frac{\mu}{K}\bar{u}^2. \tag{17}$$

where $S_h$ the specific heat capacity, and $T_c$ represents the thermal conductivity of the fluid. In Eq (17), the second term indicates the volumetric heat generation caused by the viscous dissipation, and the third term indicates the impact of Joule heating.

The temperature profile for the fully developed flow depends on the $\tilde{y}$ direction only, and satisfies the condition:

$$\frac{\partial}{\partial\tilde{x}}\left(\frac{\tilde{T}\left(\tilde{x},\tilde{y}\right)-\tilde{T}_s\left(\tilde{x}\right)}{\tilde{T}_m\left(\tilde{x}\right)-\tilde{T}_s\left(\tilde{x}\right)}\right)=0. \tag{18}$$

Using the boundary conditions and the above equation, we obtain the following equations:

$$\frac{\partial\tilde{T}}{\partial\tilde{x}}=\frac{d\tilde{T}_m}{d\tilde{x}}=k,\text{ and }\frac{\partial^2\tilde{T}}{\partial\tilde{x}^2}=0. \tag{19}$$

where $k$ is constant.

The energy equation with its pertinent boundary conditions may be cast in the following form:

$$\rho S_h\bar{u}\frac{\partial\tilde{T}}{\partial\tilde{x}}=T_c\frac{\partial^2\tilde{T}}{\partial\tilde{y}^2}+\mu\left(\frac{\mathrm{d}\bar{u}}{\mathrm{d}\tilde{y}}\right)\frac{\left[\frac{\mathrm{d}\bar{u}}{\mathrm{d}\tilde{y}}+\beta_1\left(\frac{\mathrm{d}\bar{u}}{\mathrm{d}\tilde{y}}\right)^3\right]}{\left[1+\beta_2\left(\frac{\mathrm{d}\bar{u}}{\mathrm{d}\tilde{y}}\right)^2\right]}+\sigma\left(E^2+B^2\bar{u}^2-2EB\bar{u}\right)+\frac{\rho c_F}{K^{1/2}}\bar{u}^3+\frac{\mu}{K}\bar{u}^2, \tag{20}$$

$$Q_s=T_c\left.\frac{\partial\tilde{T}}{\partial\tilde{y}}\right|_{\tilde{y}=\pm H}\quad\text{or}\quad\left.\tilde{T}\right|_{\bar{y}=\pm H}=\tilde{T}_s\left(\tilde{x}^2\right), \tag{21}$$

where $Q_s$ represents the constant heat flux at the wall. For the geometric configuration examined here, the energy equation for an infinitesimal section with length $\mathrm{d}\tilde{x}$ becomes:

$$\rho S_h \bar{u}_m H \mathrm{d}\tilde{T}_m = Q_s \mathrm{d}\tilde{x} + \sigma H E^2 \mathrm{d}\tilde{x} + \sigma \int_0^H B\left(B\bar{u}^2 - 2E\bar{u}\right)\mathrm{d}\tilde{y}\mathrm{d}\tilde{x}$$
$$+ \mu \int_0^H \left[\frac{\mathrm{d}\bar{u}}{\mathrm{d}\tilde{y}} + \beta_1\left(\frac{\mathrm{d}\bar{u}}{\mathrm{d}\tilde{y}}\right)^3\right]\left[1 + \beta_2\left(\frac{\mathrm{d}\bar{u}}{\mathrm{d}\tilde{y}}\right)^2\right]^{-1}\left(\frac{\mathrm{d}\bar{u}}{\mathrm{d}\tilde{y}}\right)^2 \mathrm{d}\tilde{y}\mathrm{d}\tilde{x} + \int_0^H \left(\frac{\rho c_F}{K^{1/2}}\bar{u}^3 + \frac{\mu}{K}\bar{u}^2\right)\mathrm{d}\tilde{y}\mathrm{d}\tilde{x}. \tag{22}$$

Hence, the mean temperature may be written as follows:

$$\frac{d\tilde{T}_m}{d\tilde{x}} = \frac{C_0}{\rho S_h} = \text{constant} \tag{23}$$

where,

$$C_0 = \frac{Q_s}{C_1} + \frac{\sigma E^2 H}{C_1} + \frac{\sigma B^2 C_2}{C_1} + \frac{\mu C_3}{C_1} + \frac{C_4}{C_1} - 2BE\sigma, \tag{24}$$

The coefficients of the previous equations that are used in the calculations are:

$$C_1 = \int_0^H \bar{u}\mathrm{d}\tilde{y}, C_2 = \int_0^H \bar{u}^2 \mathrm{d}\tilde{y}, C_3 = \int_0^H \left[\frac{\mathrm{d}\bar{u}}{\mathrm{d}\tilde{y}} + \beta_1\left(\frac{\mathrm{d}\bar{u}}{\mathrm{d}\tilde{y}}\right)^3\right]\left[1 + \beta_2\left(\frac{\mathrm{d}\bar{u}}{\mathrm{d}\tilde{y}}\right)^2\right]^{-1}\left(\frac{\mathrm{d}\bar{u}}{\mathrm{d}\tilde{y}}\right)^2 \mathrm{d}\tilde{y},$$
$$C_4 = \int_0^H \left(\frac{\rho c_F}{K^{1/2}}\bar{u}^3 + \frac{\mu}{K}\bar{u}^2\right)\mathrm{d}\tilde{y}, \tag{25}$$

The energy equation, Eq (20), and its boundary conditions become in dimensionless form:

$$\frac{\mathrm{d}^2 T}{\mathrm{d}y^2} + Bm\left(\frac{\mathrm{d}u}{\mathrm{d}y}\right)^2 \frac{\left[1 + \xi_1\left(\frac{\mathrm{d}u}{\mathrm{d}y}\right)^2\right]}{\left[1 + \xi_2\left(\frac{\mathrm{d}u}{\mathrm{d}y}\right)^2\right]} - \xi_3 u + Bm \times Ha^2 u^2 + \xi_4 + Da \times Bm \times u^2 + Bm \times F \times u^3 = 0, \tag{26}$$

$$T(y) = 0, \quad y = \pm 1, \tag{27}$$

where $Bm$ is the Brinkman number –the ratio of heat produced because of viscous dissipation to the conduction heat transfer; $\xi_1$ and $\xi_2$ are defined in Eq (14); $\xi_3$ represents the ratio of the Joule heating to the heat conduction; and $\xi_4$ represents the influence of heat generation because of the influence of the electric and magnetic fields to the heat conduction. These dimensionless parameters are expressed as follows:

$$Bm = \frac{\mu \upsilon^2}{H^2 T_c\left(\tilde{T}_m - \tilde{T}_s\right)}, \xi_3 = \frac{\upsilon\left(2\sigma EB + C_0\right)H}{T_c\left(\tilde{T}_m - \tilde{T}_s\right)}, \xi_4 = \frac{\sigma E^2 H^2}{T_c\left(\tilde{T}_m - \tilde{T}_s\right)}. \tag{28}$$

The Nusselt number, which denotes the effects of convective heat transfer, is written as follows:

$$Nu = \frac{h_c D_H}{T_c} = \frac{D_H Q_s}{T_c\left(\tilde{T}_s - \tilde{T}_m\right)}, \tag{29}$$

where $Q_s = h_c\left(\tilde{T}_s - \tilde{T}_m\right)$, and $h_c$ is the coefficient of convective heat transfer and, $D_H\left(=H\right)$ denotes the hydrodynamics diameter of the microchannel. Using Eqs (21) and (29), the final form of the Nusselt number at the upper wall is expressed as:

$$Nu = -\left.\frac{\mathrm{d}T}{\mathrm{d}y}\right|_{y=1}. \tag{30}$$

## 3. Solutions of the governing equations

Because the final forms of Eqs (15) and (26) are nonlinear, closed-form solutions cannot be obtained. Thus, a numerical scheme is proposed to obtain the solution of the equations. The shooting method is the most effective scheme to solve nonlinear differential equations. To use this numerical scheme, we first reduce Eqs (15) and (26) to first-order differential equation systems and then solve them using the numerical algorithm developed in Mathematica. This technique is advantageous to other similar methods, because it produces better results in a shorter period [29–31]. As a result, Eqs (15) and (26) are reduced to the following form:

$$\left.\begin{aligned} &\frac{\mathrm{d}u}{\mathrm{d}y} = F_1, \frac{\mathrm{d}^2u}{\mathrm{d}y^2} = F_1' = F_2, \\ &F_2 + \left(3\xi_1 - \xi_2\right)F_2F_1^2 + \xi_1\xi_2F_2F_1^4 - \left(Ha^2 \times u - E_1 + Da \times u + F \times u^2 - Gr \times T\right)\left[1 + \xi_2F_1^2\right]^2 = 0, \end{aligned}\right\} \tag{31}$$

$$\left.\begin{aligned} &\frac{\mathrm{d}T}{\mathrm{d}y} = G_1, \frac{\mathrm{d}^2T}{\mathrm{d}y^2} = G_1' = G_2, \\ &G_2 + Bm\left(F_1\right)^2\left(\frac{1+\xi_1F_1^2}{1+\xi_2F_1^2}\right) - \xi_3u + Bm \times Ha^2u^2 + \xi_4 + Da \times Bm \times u^2 + Bm \times F \times u^3 = 0, \end{aligned}\right\} \tag{32}$$

The boundary conditions are:

$$u\left(y\right) = 0, T\left(y\right) = 0, \qquad \text{at} \qquad y = \pm 1, \tag{33}$$

## 4. Graphical and numerical analysis

This section focuses on the graphical presentation of the numerical results as affected by all the variation of the important parameters for flow and heat transfer. In particular, we investigate the behavior of the velocity profile, the Nusselt number, and the temperature profile. The following parametric values are chosen in the calculations: the semi-height of the geometric domain is in the range $H = 100 - 200\ \mu\mathrm{m}$; the range of the imposed magnetic field is $0.018 - 0.44\mathrm{T}$; the values of the Hartman number are in the range $0.8 \times 10^{-6}$ to $3$; the value of the imposed electric field strength is $1 \times 60\mathrm{V/m}$; the dimensionless parameter $E_1$ is in the range $0.4 \times 10^{-8}$ to $2.1 \times 10^{5}$; The Brinkman

number is $Bm = 10.5$; the Oldroyd 6-constant fluid parameters are $\xi_1 = 1, \xi_2 = 0.5;$ the Darcy-Brinkman-Forchheimer parameter is $F = 1;$ and the thermal Grashof number is $Gr = 0.2.$ It must be noted that the results for a simply viscous Newtonian fluid can easily recovered in this model by setting $\xi_1 = \xi_2 = 0$.

Table 1 shows the computational results of the Nusselt number against all the important parameters of this problem.

**Table 1.** Nusselt number computational results for all emerging parameters.

| $\xi_1$ | $\xi_2$ | $\xi_3$ | $Ha$ | $F$ | $Da$ | $Gr$ | $Bm$ | $Nu$ |
|---|---|---|---|---|---|---|---|---|
| 1 | 0.5 | 2.5 | 1 | 0.5 | 0.5 | 0.2 | 10.5 | 2.640184 |
| 2 | | | | | | | | 2.406574 |
| | 1 | | | | | | | 2.844562 |
| | 3 | | | | | | | 4.401719 |
| | | 2 | | | | | | 2.809293 |
| | | 3 | | | | | | 2.475700 |
| | | | 0.5 | | | | | 3.014919 |
| | | | 0.8 | | | | | 2.812321 |
| | | | | 0.8 | | | | 2.767278 |
| | | | | 1 | | | | 2.740628 |
| | | | | | 0.6 | | | 2.759587 |
| | | | | | 0.7 | | | 2.732662 |
| | | | | | | 0.1 | | 2.282343 |
| | | | | | | 0.15 | | 2.442868 |
| | | | | | | | 6 | 1.313252 |
| | | | | | | | 7 | 1.573756 |

Figure 1 is a schematic representation of the micro-pumps, showing the dimensions and the direction of the heat transfer. Figure 2 shows the results of the Nusselt number in graphical/column form. It is clearly observed in this Figure that the Nusselt number is suppressed due to the strong impact of Hartmann number $Ha$, Darcy parameter $Da$, and the fluid parameter $\xi_1$. However, the Nusselt number increases with the Brinkman number $Bm$, the thermal Grashof number $Gr$, and the fluid parameter $\xi_2$.

Figure 3 is plotted for the velocity profile to show the behavior of the fluid parameters $\xi_1$ and $\xi_2$. One can see in this Figure that increasing the values of $\xi_1$ suppress the magnitude of the velocity. On the other hand, the fluid parameter $\xi_2$ acts in reverse and increases the velocity. The solid line corresponds to the case of a viscous fluid.

The impact of the buoyancy forces on the working fluid is represented by the thermal Grashof number. Figure 4 shows the variation of the thermal Grashof number, $Gr$, and is effects on the fluid velocity. The thermal Grashof number augments the velocity profile along the entire channel, as shown in this graph.

The effects of the Darcy-Brinkman-Forchheimer parameter, $F$, is shown in Figure 5. It is apparent that increasing $F$ significantly retards the flow. A similar behavior was observed in the viscous fluid flows through a Riga plate [32].

Figure 6 shows the influence of the Hartmann number, *Ha*, on the fluid velocity. The existence of an external magnetic field introduces resistance to the fluid flow, as it is apparent in the Figure. The resistance is caused by the Lorentz force, which is a consequence of the combined application of the electric and magnetic fields. The case $Ha = 0$ corresponds to the absence of the magnetic field and the velocity profile attains its maximum. As expected, the velocity field is also retarded with the Darcy parameter, *Da*, whose influence is plotted in Figure 7. The effects of the parameters *Ha* and *Da* are very similar on the entire velocity profile. Figure 8 shows the variation of electric field $E_1$ strength on the velocity profile. It is observed in the Figure that increasing values of the electric field enhances the velocity profile, since electric field produces larger aiding forces which boost the velocity profile.

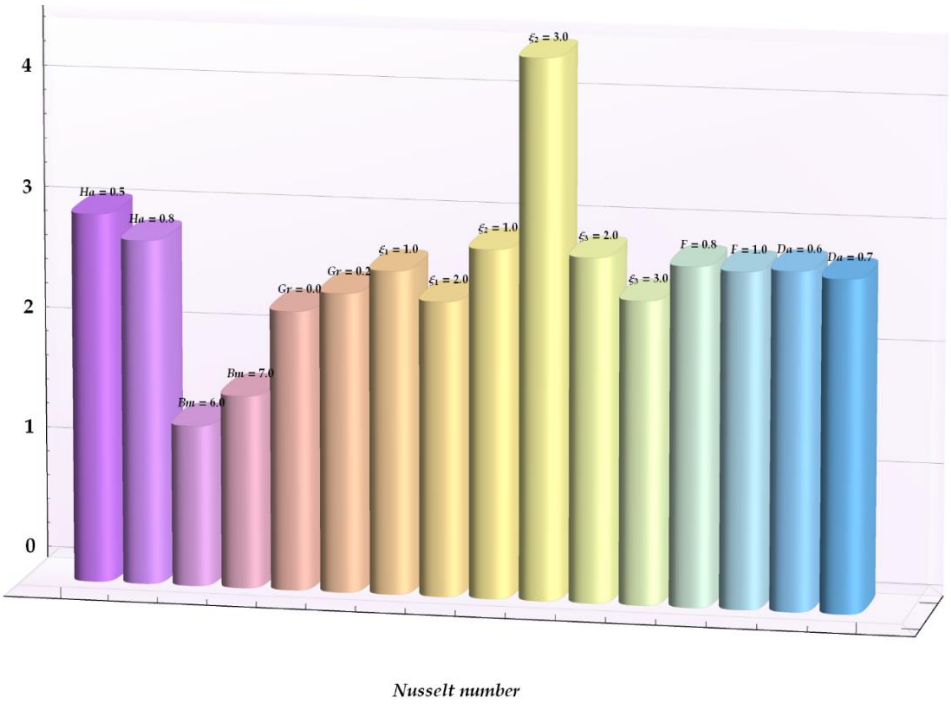


**Figure 2.** Nusselt number variation on the upper wall for several of the governing equations parameters.

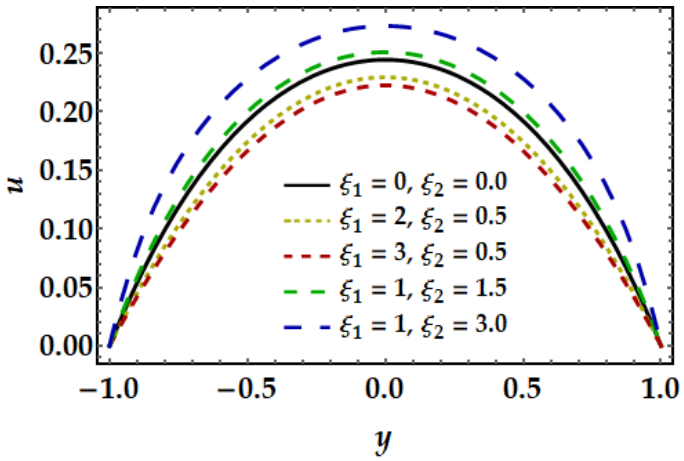


**Figure 3.** Effect of the $\xi_1$ and $\xi_2$ variation on the velocity profile.

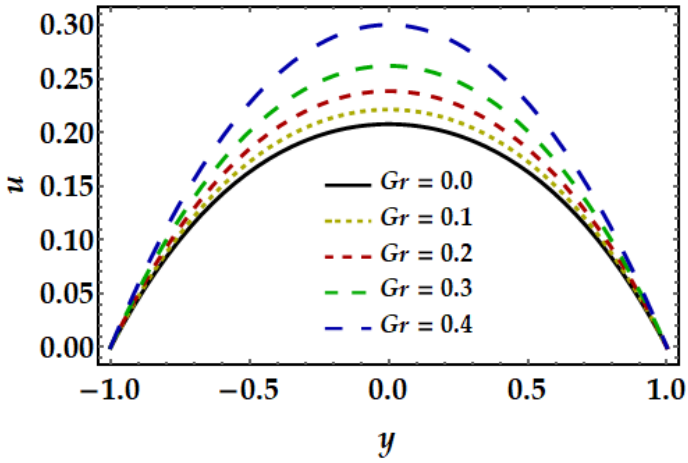


**Figure 4.** Effect of the $Gr$ variation on the velocity profile.

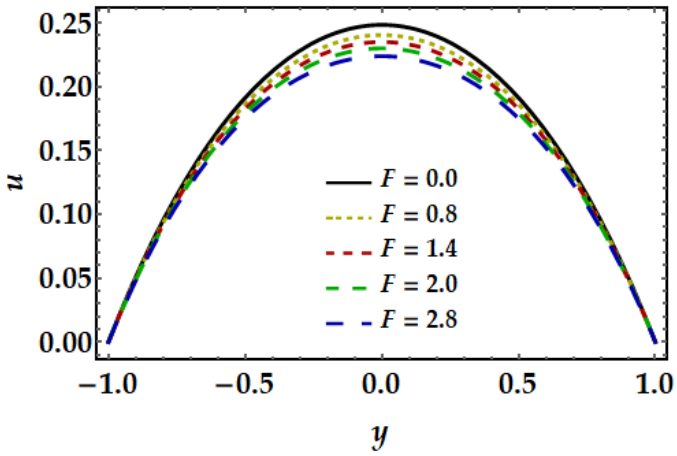


**Figure 5.** Effect of the parameter $F$ variation on the velocity profile.

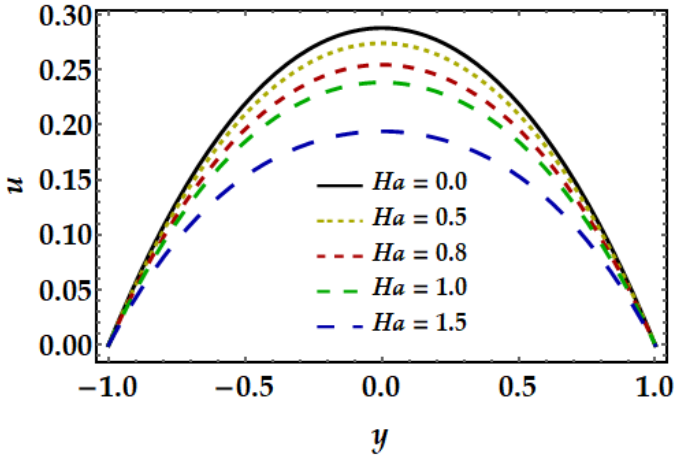


**Figure 6.** Effect of the $Ha$ variation on the velocity profile.

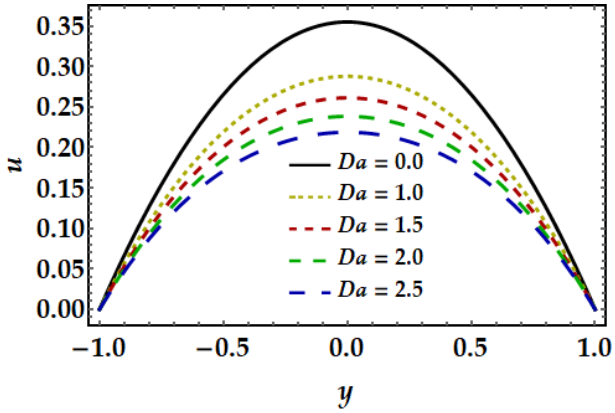


**Figure 7.** Effect of the *Da* variation on the velocity profile.

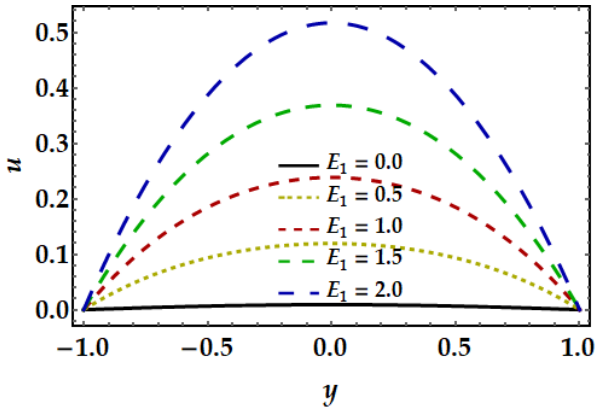


**Figure 8.** Effect of the $E_1$ variation on the velocity profile.

Figures 9–16 depict the effect of the several parameters on the temperature profile. As shown in Figure 9, the Brinkman number *Bm*, which is the product of the Prandtl number and the Eckert number, enhances the temperature profile. The higher values of the Brinkman number impede the heat diffusion caused by the viscous dissipation, causing the temperature profile to grow.

Figure 10 shows the effect of the fluid parameters $\xi_1$ and $\xi_2$. It is observed that the variation of the two parameters affects very little the temperature profile. In contrast, the variation of the Grashof number has a very significant effect on the temperature profile as shown in Figure 11.

The variation of the Darcy-Brinkman-Forchheimer parameter, *F*, on the temperature profile is shown in Figure 12, where it may be seen that increasing *F* has a small but detrimental effect on the temperature profile. Figure 13 shows that the magnetic field parameter, *Ha*, diminishes the temperature profile. This effect also causes significant entropy production and exergy destruction [33]. On the contrary, the temperature profile was dramatically decreased at the larger values of the parameter $\xi_3$, as it may be observed in Figure 14. The effect of the Darcy number, *Da*, is similar since it lowers the temperature profile, as it is shown in Figure 15. It may be concluded from the last two cases, that increasing the parameters $\xi_3$ and *Da* reduces the thermal dissipation and exergy destruction [33]. The last Figure 16 shows the variation of the electric field strength on the temperature profile. It can be seen that larger values $E_1$ cause significant increment of the temperature profile. It must be noted that the case $E_1 = 0$ corresponds to the absence of electric field and its influence on the flow regime.

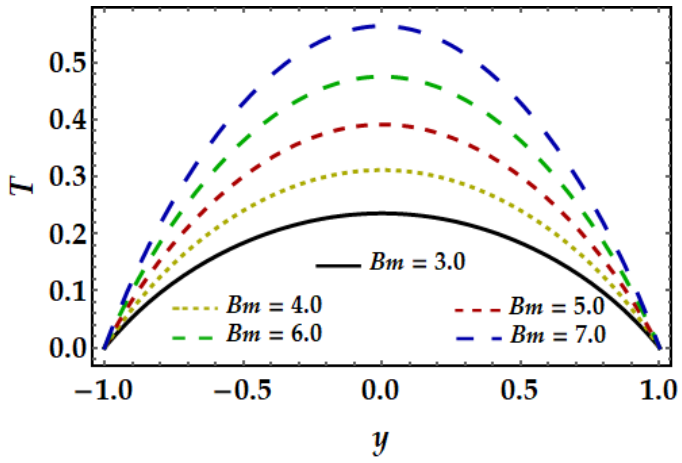


**Figure 9.** Effect of the $Bm$ variation on the temperature profile.

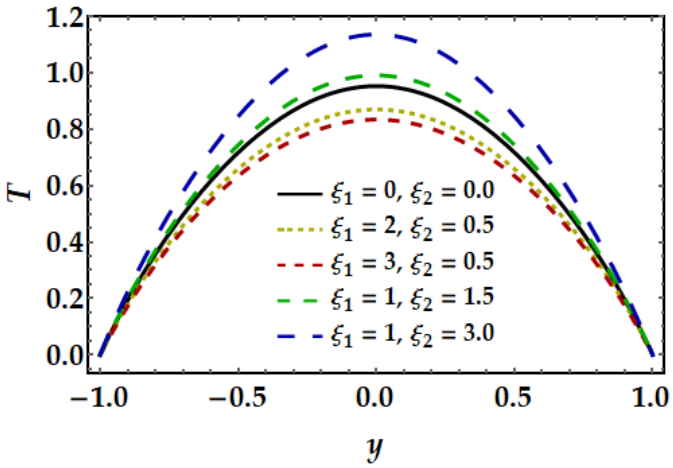


**Figure 10.** Effect of the variation of the parameters $\xi_1$ *and* $\xi_2$ on the temperature profile.

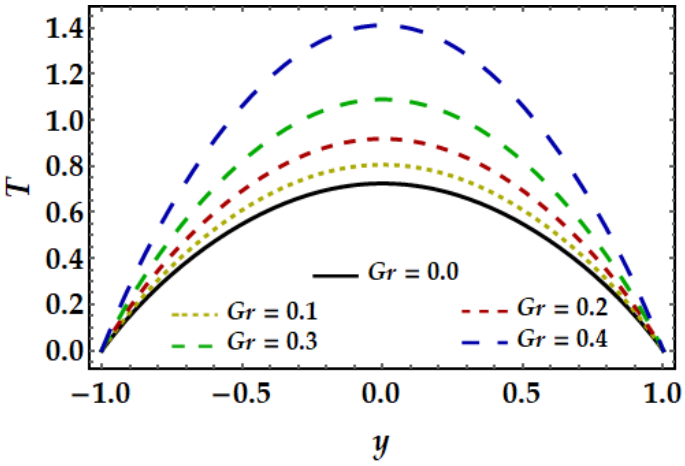


**Figure 11.** Effect of the *Gr* variation on the temperature profile.

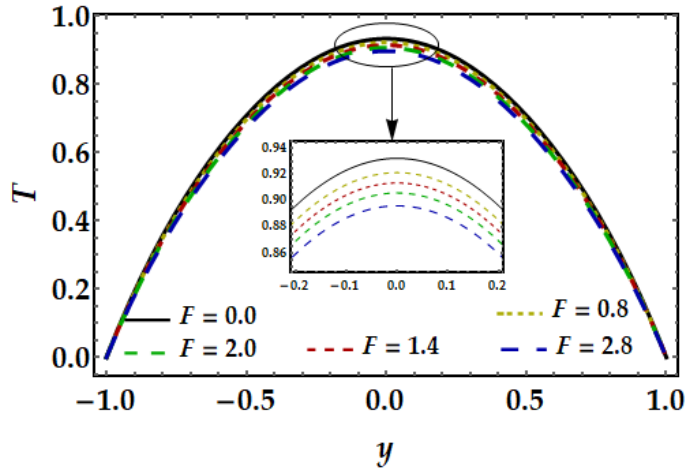


**Figure 12.** Effect of the $F$ variation on the temperature profile.

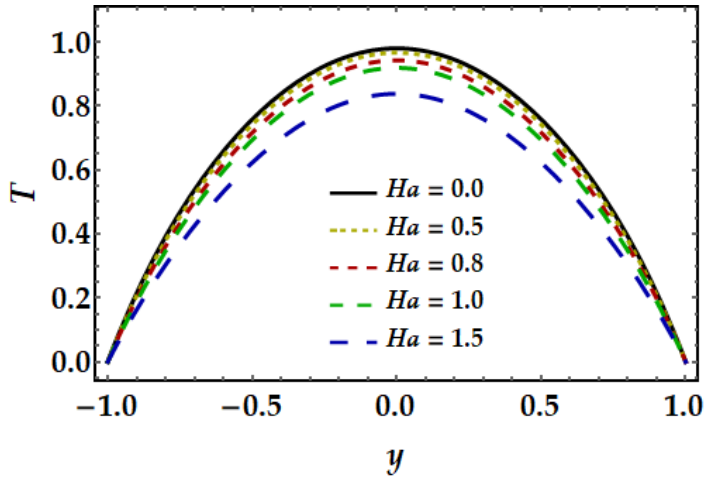


**Figure 13.** Effect of the $Ha$ variation on the temperature profile.

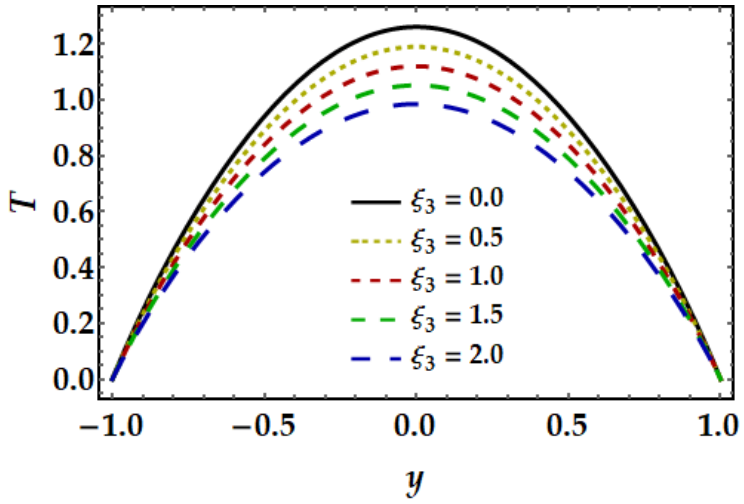


**Figure 14.** Effect of the $\xi_3$ variation on the temperature profile.

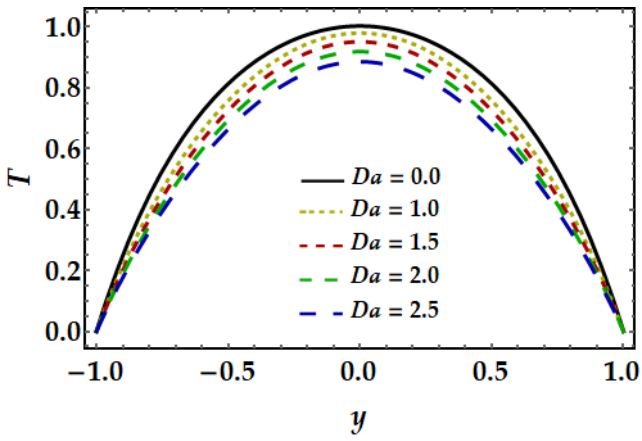


**Figure 15.** Effect of the *Da* variation on the temperature profile.

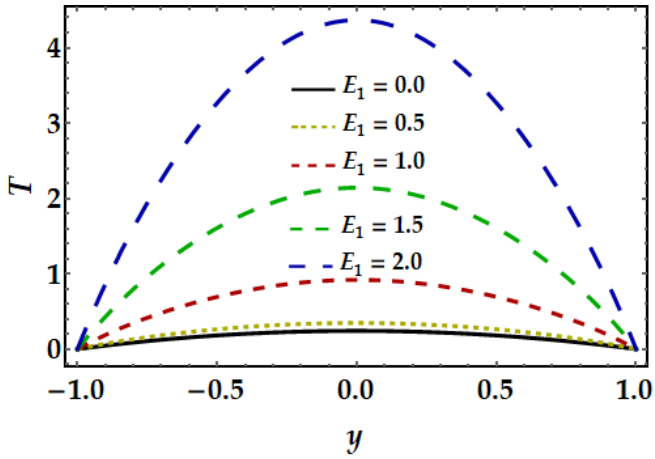


**Figure 16.** Effect of the $E_1$ variation on the temperature profile.

## 5. Conclusions

The Darcy-Brinkman-Forchheimer model was used to investigate the behavior of an Oldroyd 6-constant fluid in an electro-magneto-hydrodynamic fluid flow through parallel micro-plates with heat transfer. The effects of the viscous dissipation and Joule heating are considered in the model. The governing equations for this type of fluid are nonlinear and coupled, which implies that exact solutions are not possible to obtain. Hence, we used the shooting method to obtain numerical solutions. The governing equations are first developed and then cast in dimensionless form. With the results of the numerical solution and the effects of all the pertinent dimensionless variables are discussed using graphs and tables. The following are the key conclusions of the study:

i. The Nusselt number increases with the Brinkmann and Grashof numbers, but decreases with the Hartmann number.

ii. The Grashof number significantly increases the fluid velocity, but the Darcy parameter and the magnetic field, which creates the Lorenz force impede the fluid motion.

iii. The Oldroyd 6-constant fluid parameters affect both the velocity and temperature profiles, but their effects on the temperature profile are very small.

The Darcy-Brinkman-Forchheimer parameter slightly decreases the temperature profile. The parameter associated with the magnetic field, *Ha,* acts to increase the temperature profile.

## Conflict of interest

The authors declare no conflict of interest.

## References


1. D. A. Konovalov, V. I. Ryazhskikh, I. N. Lazarenko, N. N. Kozhukhov, Model of cooling of compact surfaces by microchannel recuperative heat exchangers with a matrix of filamentary silicon single crystals, *J. Eng. Phys. Thermophys.*, **92** (2019), 355–364. https://doi.org/10.1007/s10891-019-01938-2
2. K. Nakatsuka, B. Jeyadevan, S. Neveu, H. Koganezawa, The magnetic fluid for heat transfer applications, *J. Magn. Magn. Mater.*, **252** (2002), 360–362. https://doi.org/10.1016/s0304-8853(02)00683-2
3. L. Theodore, *Heat transfer applications for the practicing engineer*, Hoboken, NJ: Wiley-Blackwell, 2011. https://doi.org/10.1002/9780470937228
4. H. Singh, R. S. Myong, Critical review of fluid flow physics at micro- to nano-scale porous media applications in the energy sector, *Adv. Mater. Sci. Eng.*, **2018** (2018), 9565240. https://doi.org/10.1155/2018/9565240
5. A. Moradi, D. Toghraie, A. H. M. Isfahani, A. Hosseinian, An experimental study on MWCNT–water nanofluids flow and heat transfer in double-pipe heat exchanger using porous media, *J. Therm. Anal. Calorim.*, **137** (2019), 1797–1807. https://doi.org/10.1007/s10973-019-08076-0
6. I. Ataei-Dadavi, M. Chakkingal, S. Kenjeres, C. R. Kleijn, M. J. Tummers, Flow and heat transfer measurements in natural convection in coarse-grained porous media, *Int. J. Heat Mass Tran.*, **130** (2019), 575–584. https://doi.org/10.1016/j.ijheatmasstransfer.2018.10.118
7. N. S. Pandya, H. Shah, M. Molana, A. K. Tiwari, Heat transfer enhancement with nanofluids in plate heat exchangers: A comprehensive review, *Eur. J. Mech. B Fluid*., **81** (2020), 173–190. https://doi.org/10.1016/j.euromechflu.2020.02.004
8. S. M. Miri Joibary, M. Siavashi, Effect of Reynolds asymmetry and use of porous media in the counterflow double-pipe heat exchanger for passive heat transfer enhancement, *J. Therm. Anal. Calorim.*, **140** (2020), 1079–1093. https://doi.org/10.1007/s10973-019-08991-2
9. L. Zhang, M. M. Bhatti, R. Ellahi, E. E. Michaelides, Oxytactic microorganisms and thermo-bioconvection nanofluid flow over a porous riga plate with Darcy–Brinkman–Forchheimer medium, *J. Non-Equilib. Thermodyn.*, **45** (2020), 257–268. https://doi.org/10.1515/jnet-2020-0010
10. F. Selimefendigil, H. F. Öztop, Combined effects of double porous layers and nanofluids on the performance of confined single and multi-jet impingement heat transfer, *Chem. Eng. Commun.*, **209** (2022), 925–937. https://doi.org/10.1080/00986445.2021.1928650
11. J. West, B. Karamata, B. Lillis, J. P. Gleeson, J. Alderman, J. K. Collins, et al., Application of magnetohydrodynamic actuation to continuous flow chemistry, *Lab Chip.*, **2** (2002), 224–230. https://doi.org/10.1039/b206756k

12. M. Yi, S. Qian, H. H. Bau, A magnetohydrodynamic chaotic stirrer, *J. Fluid Mech.*, **468** (2002), 153–177. https://doi.org/10.1017/s0022112002001635
13. N. Pamme, Magnetism and microfluidics, *Lab Chip.*, **6** (2006), 24–38. https://doi.org/10.1039/b513005k
14. N. T. Nguyen, Micro-magnetofluidics: interactions between magnetism and fluid flow on the microscale, *Microfluid. Nanofluidics*., **12** (2012), 1–16. https://doi.org/10.1007/s10404-011-0903-5
15. M. M. Bhatti, A. Zeeshan, M. A. Asif, R. Ellahi, S. M. Sait, Non-uniform pumping flow model for the couple stress particle-fluid under magnetic effects, *Chem. Eng. Commun*., **209** (2022), 1058–1069. https://doi.org/10.1080/00986445.2021.1940156
16. R. Chakraborty, R. Dey, S. Chakraborty, Thermal characteristics of electromagnetohydrodynamic flows in narrow channels with viscous dissipation and Joule heating under constant wall heat flux, *Int. J. Heat Mass Trans.*, **67** (2013), 1151–1162. https://doi.org/10.1016/j.ijheatmasstransfer.2013.08.099
17. S. Sarkar, S. Ganguly, S. Chakraborty, Influence of combined electromagnetohydrodynamics on microchannel flow with electrokinetic effect and interfacial slip, *Microfluid. Nanofluidics.*, **21** (2017), 56. https://doi.org/10.1007/s10404-017-1894-7
18. M. Rashid, S. Nadeem, I. Shahzadi, Permeability impact on electromagnetohydrodynamic flow through corrugated walls of microchannel with variable viscosity, *Adv. Mech. Eng.*, **12** (2020), 1–11. https://doi.org/10.1177/1687814020944336
19. M. Reza, A. Rana, G. C. Shit, Thermo-fluidic transport of electromagnetohydrodynamic flow in a corrugated porous medium microchannel, *Eur. Phys. J. Plus*, **136** (2021), 496. https://doi.org/10.1140/epjp/s13360-021-01505-w
20. M. Reza, A. Rana, R. Patra, A numerical experiment on Thermo-fluidic transport of third-grade fluid flow through a porous microchannel under the influence of combined electromagnetohydrodynamic effect, In: *Advances in mechanical processing and design*, Singapore: Springer, 2021, 115–126. https://doi.org/10.1007/978-981-15-7779-6_10
21. A. M. Obalalu, O. A. Ajala, A. O. Akindele, S. Alao, A. Okunloye, Effect of melting heat transfer on electromagnetohydrodynamic non-newtonian nanofluid flow over a riga plate with chemical reaction and arrhenius activation energy, *Eur. Phys. J. Plus*, **136** (2021), 891. https://doi.org/10.1140/epjp/s13360-021-01869-z
22. D. J. Laser, J. G. Santiago, A review of micropumps, *J. Micromech. Microeng.*, **14** (2004), R35–R64. https://doi.org/10.1088/0960-1317/14/6/r01
23. H. A. Stone, A. D. Stroock, A. Ajdari, Engineering flows in small devices: Microfluidics toward a lab-on-a-chip, *Annu. Rev. Fluid Mech.*, **36** (2004), 381–411. https://doi.org/10.1146/annurev.fluid.36.050802.122124
24. M. M. Bhatti, O. A. Bég, R. Ellahi, T. Abbas, Natural convection non-Newtonian EMHD dissipative flow through a microchannel containing a non-Darcy porous medium: Homotopy perturbation method study, *Qual. Theory Dyn. Syst.*, **21** (2022), 97. https://doi.org/10.1007/s12346-022-00625-7
25. P. Liang, S. Wang, M. Zhao, Numerical study of rotating electroosmotic flow of Oldroyd-B fluid in a microchannel with slip boundary condition, *Chinese J. Phys.*, **65** (2020), 459–471. https://doi.org/10.1016/j.cjph.2020.02.025

26. X. Wang, H. Xu, H. Qi, Transient magnetohydrodynamic flow and heat transfer of fractional Oldroyd-B fluids in a microchannel with slip boundary condition, *Phys. Fluids*, **32** (2020), 103104. https://doi.org/10.1063/5.0025195
27. S. O. Salawu, A. B. Disu, Branch-chain criticality and thermal explosion of Oldroyd 6-constant fluid for a generalized Couette reactive flow, *South African Journal of Chemical Engineering*, **34** (2020), 90–96. https://doi.org/10.1016/j.sajce.2020.06.004
28. T. Hayat, M. Khan, M. Sajid, M. Ayub, Steady flow of an Oldroyd 8-constant fluid between coaxial cylinders in a porous medium, *J. Porous Media*, **9** (2006), 709–722. https://doi.org/10.1615/jpormedia.v9.i8.10
29. M. Zhao, C. Yang, C. Fan, Q. Zhang, A shooting method for nonlinear boundary value problems in a thermal piezoelectric semiconductor plate, *Z. Angew. Math. Mech.*, **100** (2020), e201900302. https://doi.org/10.1002/zamm.201900302
30. I. K. Argyros, J. Ceballos, D. González, J. M. Gutiérrez, Extending the applicability of Newton's method for a class of boundary value problems using the shooting method, *Appl. Math. Comput.*, **384** (2020), 125378. https://doi.org/10.1016/j.amc.2020.125378
31. A. Daneshyar, P. Sotoudeh, M. Ghaemian, A shooting approach to the scaled boundary finite element equations of elastodynamics in the frequency domain, *Comput. Method. Appl. Mech. Eng.*, **387** (2021), 114170. https://doi.org/10.1016/j.cma.2021.114170
32. B. Q. Zhao, A. Pantokratoras, T. G. Fang, S. J. Liao, Flow of a weakly conducting fluid in a channel filled with a Darcy–Brinkman–forchheimer porous medium, *Transp. Porous Med.*, **85** (2010), 131–142. https://doi.org/10.1007/s11242-010-9550-7
33. E. Michaelides, *Exergy analysis for energy conversion systems*, Cambridge, England: Cambridge University Press, 2021. https://doi.org/10.1017/9781108635684

## Appendix

The scalar forms (time-dependent) of Eq (5) are found as:

$$\xi_{\tilde{x}\tilde{x}} + \lambda_1\left(\frac{\partial}{\partial\tilde{t}}\xi_{\tilde{x}\tilde{x}} - 2\xi_{\tilde{x}\tilde{y}}\frac{\partial\bar{u}}{\partial\tilde{y}}\right) + \lambda_3\xi_{\tilde{x}\tilde{y}}\frac{\partial\bar{u}}{\partial\tilde{y}} = \mu\left(\lambda_4 - 2\lambda_2\right)\left(\frac{\partial\bar{u}}{\partial\tilde{y}}\right)^2, \tag{A1}$$

$$\xi_{\tilde{x}\tilde{y}} + \lambda_1\left(\frac{\partial}{\partial\tilde{t}}\xi_{\tilde{x}\tilde{y}} - \xi_{\tilde{y}\tilde{y}}\frac{\partial\bar{u}}{\partial\tilde{y}}\right) + \left(\frac{\lambda_3+\lambda_5}{2}\right)\left(\xi_{\tilde{x}\tilde{x}} + \xi_{\tilde{y}\tilde{y}}\right)\frac{\partial\bar{u}}{\partial\tilde{y}} + \frac{\lambda_5}{2}\xi_{\tilde{z}\tilde{z}}\frac{\partial\bar{u}}{\partial\tilde{y}} = \mu\frac{\partial\bar{u}}{\partial\tilde{y}} + \mu\lambda_2\frac{\partial^2\bar{u}}{\partial\tilde{t}\,\partial\tilde{y}}, \tag{A2}$$

$$\xi_{\tilde{z}\tilde{x}} + \lambda_1\left(\frac{\partial}{\partial\tilde{t}}\xi_{\tilde{z}\tilde{x}} - \xi_{\tilde{z}\tilde{y}}\frac{\partial\bar{u}}{\partial\tilde{y}}\right) + \frac{\lambda_3}{2}\xi_{\tilde{z}\tilde{y}}\frac{\partial\bar{u}}{\partial\tilde{y}} = 0, \tag{A3}$$

$$\xi_{\tilde{y}\tilde{y}} + \lambda_1\frac{\partial}{\partial\tilde{t}}\xi_{\tilde{y}\tilde{y}} + \lambda_3\xi_{\tilde{x}\tilde{y}}\frac{\partial\bar{u}}{\partial\tilde{y}} = \mu\lambda_4\left(\frac{\partial\bar{u}}{\partial\tilde{y}}\right)^2, \tag{A4}$$

$$\xi_{\tilde{z}\tilde{y}} + \lambda_1\frac{\partial}{\partial\tilde{t}}\xi_{\tilde{z}\tilde{y}} + \frac{\lambda_3}{2}\xi_{\tilde{z}\tilde{x}}\frac{\partial\bar{u}}{\partial\tilde{y}} = 0, \tag{A5}$$

$$\xi_{\tilde{z}\tilde{z}} + \lambda_1 \frac{\partial}{\partial \tilde{t}} \xi_{\tilde{z}\tilde{z}} = 0. \tag{A6}$$

The time-independent equations are as follows:

$$\xi_{\tilde{x}\tilde{x}} + (\lambda_3 - 2\lambda_1)\xi_{\tilde{x}\tilde{y}} \frac{\mathrm{d}\bar{u}}{\mathrm{d}\tilde{y}} = \mu(\lambda_4 - 2\lambda_2)\left(\frac{\mathrm{d}\bar{u}}{\mathrm{d}\tilde{y}}\right)^2, \tag{A7}$$

$$\xi_{\tilde{x}\tilde{y}} - \lambda_1 \xi_{\tilde{y}\tilde{y}} \frac{\mathrm{d}\bar{u}}{\mathrm{d}\tilde{y}} + \left(\frac{\lambda_3 + \lambda_5}{2}\right)\left(\xi_{\tilde{x}\tilde{x}} + \xi_{\tilde{y}\tilde{y}}\right)\frac{\mathrm{d}\bar{u}}{\mathrm{d}\tilde{y}} + \frac{\lambda_5}{2}\xi_{\tilde{z}\tilde{z}} \frac{\mathrm{d}\bar{u}}{\mathrm{d}\tilde{y}} = \mu \frac{\mathrm{d}\bar{u}}{\mathrm{d}\tilde{y}}, \tag{A8}$$

$$\xi_{\tilde{z}\tilde{x}} + \left(\frac{\lambda_3 - 2\lambda_1}{2}\right)\xi_{\tilde{z}\tilde{y}} \frac{\mathrm{d}\bar{u}}{\mathrm{d}\tilde{y}} = 0, \tag{A9}$$

$$\xi_{\tilde{y}\tilde{y}} + \lambda_3 \xi_{\tilde{x}\tilde{y}} \frac{\mathrm{d}\bar{u}}{\mathrm{d}\tilde{y}} = \mu\lambda_4 \left(\frac{\mathrm{d}\bar{u}}{\mathrm{d}\tilde{y}}\right)^2, \tag{A10}$$

$$\xi_{\tilde{z}\tilde{y}} + \frac{\lambda_3}{2}\xi_{\tilde{z}\tilde{x}} \frac{\mathrm{d}\bar{u}}{\mathrm{d}\tilde{y}} = 0, \tag{A11}$$

$$\xi_{\tilde{z}\tilde{z}} = 0. \tag{A12}$$